INFLUENCE OF RESTORING-FORCE CHARACTERISTICS OF BRACES ON DYNAMIC RESPONSE OF BRACED FRAME

Michio SHIBATA[I]

SYNOPSIS

Dynamic response analysis of a single-story braced frame is presented. The hysteretic characteristics of the bare frame is assumed to be bi-linear, and the restoring-force of braces is evaluated by the hysteresis function proposed by the author and/or computed by the detailed numerical method. Both results are in good agreement, and it is confirmed that the proposed restoring-force function of a single brace can be applied to the response analysis with enough accuracy.

A parametric study using the proposed function shows that the ductility response of the braced frame much depends not only on the brace slenderness but also on the strength ratio of columns to braces.

INTRODUCTION

Braces play an important role on the earthquake resistant property of a steel structure. So, it has been desired to develope the simple and accurate mathematical expression, which approximates well the actual hysteretic behavior of steel braces. Formulated expressions should realize the following properties: 1) The axial force of a single brace subjected to random displacement history is explained as the explicit function of the axial displacement, and 2) the deterioration of strength and rigidity during the repeated loading, which is characteristic of steel braces, is precisely estimated. The author and others proposed the mathematical expression of the hysteretic rule of a single-brace at the 6 WCEE (1), which seems to satisfy the above mentioned properties better than other proposals. Although it was confirmed that the proposed formula well approximates the static test results of single brace under alternately repeated load, it must be certified that the proposed function can be applied to the dynamic response analysis with enough accuracy.

In this paper, dynamic response analysis of a single-story braced frame is presented where the hysteretic characteristics of braces is evaluated by the detailed numerical analysis (2), and the results are compared with the solution where the restoring-force of the brace is estimated by the proposed hysteresis function. A parametric study using the proposed function is also performed and the influence of the restoring-force characteristics on the maximum response is discussed.

HYSTERETIC BEHAVIOR OF A SINGLE BRACE

Formulated loop Based on the proposed hysteresis function (1), shown in Fig. 1, the non-dimensional axial force n of the brace is expressed as the single-valued continuous function of the non-dimensional axial displacement δ, untill the next unloading occurs, provided that the characteristic points A, B, P and Q, in Fig. 2, are determined at the latest unloading point.

I Lecturer, Department of Architecture, Osaka Institute of Technology.

$$n = \begin{cases} -f_c(\delta^B + n_o - \delta) & : \delta \leqq \delta^Q, \quad \dot{\delta} < 0 \quad [\text{Stage C}] \\ n^Q + (\delta - \delta^Q)\cdot\dfrac{n^P - n^Q}{\delta^P - \delta^Q} & : \delta^Q < \delta < \delta^P \quad [\text{Stage D}] \\ f_t(\delta^A - \delta) & : \delta^P \leqq \delta < \delta^A, \quad \dot{\delta} > 0 \quad [\text{Stage B}] \\ 1 & : \delta^A \leqq \delta, \quad \dot{\delta} > 0 \quad [\text{Stage A}] \end{cases} \tag{1}$$

$$f_t(x) = (p_1\cdot x + 1)^{-3/2}, \quad f_c(x) = (p_2\cdot x + p_3)^{-1/2}$$

$$p_1 = 1/(3.1\cdot n_E + 1.4), \quad p_2 = (10/n_E - 1)/3 \geqq 0, \quad p_3 = 4/n_E + 0.6 \geqq 1$$

where n_E is the ratio of the Euler load of the brace to the limit axial force, and n_o is the solution of the following equation.

$$p_2\cdot n_o^3 + p_3\cdot n_o^2 - 1 = 0 \tag{2}$$

At the unloading point, the characteristic points A, B, P, Q and the auxiliary characteristic points C and D in Figs. 3(a),(b) should be defined again. Fig. 3(a) shows the case of the unloading at Stage B,

$$\delta^A = \delta^C$$

$$\delta^B_{new} = \delta^B_{old} + (\delta^A - 1 - n_o - \delta^B_{old})\cdot(\delta - \delta^P_{old})/(\delta^A - \delta^P_{old})$$

$$\delta^P_{new} = \delta, \quad n^P_{new} = n$$

$$\delta^Q_{new} = \delta^D = \delta^B_{new} - (\delta^A - \delta)/q_1, \quad n^Q_{new} = -f_c(\delta^B_{new} + n_o - \delta^Q_{new})$$

the case of the unloading at Stage C is shown in Fig. 3(b),

$$\delta^C = \delta^A + \ln\{q_2\cdot(\delta^D - \delta) + 1\} - q_3\cdot(\delta^B - \delta^D) \geqq \delta^A$$

$$\delta^Q_{new} = \delta, \quad n^Q_{new} = n$$

$$\delta^P_{new} = \delta^C - (\delta^B - \delta)\cdot q_1, \quad n^P_{new} = f_t(\delta^C - \delta^P_{new})$$

and the case of the unloading at Stage A is expressed as follows,

$$\delta^A = \delta^P = \delta, \quad \delta^B = \delta^D = \delta^Q = \delta - 1 - n_o, \quad n^P = 1, \quad n^Q = -n_o$$

where q_1, q_2 and q_3 are the constants.

$$q_1 = 0.3\cdot\sqrt{n_E} + 0.24 \leqq 1, \quad q_2 = (3 - 1/n_E)/10, \quad q_3 = 0.115/n_E + 0.36$$

The initial values of these parameters are as follows.

$$\delta^A = \delta^C = \delta^P = n^P = 1, \quad \delta^B = \delta^D = \delta^Q = n^Q = -n_o$$

Numerical method The practical method of evaluating the precise hysteretic characteristics of a single brace (2) is summarized here. A simply supported bar is idealized into the model, shown in Fig. 4, which is composed of two straight segments and a bending portion. Assuming that the curvature of the midsection is distributed uniformly over the bending portion, the non-dimensional increment of the axial strain de of the centroid at the midsection and the non-dimensional axial-force increment dn are obtained as follows.

$$de = C_1 \cdot dk + C_2 \cdot (dk)^2/(1 + C \cdot dk) \tag{3}$$

$$dn = (C_1 \cdot \bar{A} + \rho \cdot \bar{S}) \cdot dk + C_2 \cdot \bar{A} \cdot (dk)^2/(1 + C \cdot dk) \tag{4}$$

$$C_1 = -\frac{n_c \cdot \bar{I} + \rho \cdot k \cdot \bar{S} + n}{k \cdot \bar{A} + n_c \cdot \bar{S}}, \quad C_2 = -\frac{C_1 \cdot \bar{A} + \rho \cdot \bar{S}}{k \cdot \bar{A} + n_c \cdot \bar{S}}, \quad C = \frac{\bar{A}}{k \cdot \bar{A} + n_c \cdot \bar{S}}$$

where dk is the increment of the non-dimensional curvature k of midsection, n_c is the ratio of the elastic buckling load of the model to the limit axial force, $\bar{A} = \int \mu \, dA/A$, $\bar{S} = \int y \cdot \mu \, dA/Z_p$ and $\bar{I} = \int y^2 \cdot \mu \, dA/I$ are obtained by integrating the ratio μ of the tangent modulus of each fiber element of the midsection to the Young's modulus, over the cross-sectional area, y denotes the distance of each fiber from the centroid, and $\rho = Z_p^2/(A \cdot I)$ is determined by the cross-sectional area A, the plastic section modulus Z_p and the moment of inertia I of the midsection.

In the actual calculation $\bar{A}$, $\bar{S}$ and $\bar{I}$ are computed by dividing the midsection into finite number of strip elements, assuming the uniform distribution of μ in a strip. Provided that the stress-strain relationship is piecewise linear, $\bar{A}$, $\bar{S}$ and $\bar{I}$ varies discretely with time and Eqs. 3 and 4 are valid for each period while $\bar{A}$, $\bar{S}$ and $\bar{I}$ keep constant. In order to carry out the accurate step-by-step computation, it is necessary to follow each step when the stiffness distribution of midsection changes.

The non-dimensional increment of the axial displacement of member ends is composed of three components, the elongation of the straight segments $d\delta_R$, that of the bending portion $d\delta_B$ and the axial component of the change in geometry $d\delta_G$.

$$d\delta = d\delta_R + d\delta_B + d\delta_G \tag{5}$$

$$d\delta_R = (1 - s) \cdot de_R, \quad d\delta_B = s \cdot de$$

$$d\delta_G = \rho/(6 \cdot n_c) \cdot d(k^2) = \rho/(6 \cdot n_c) \cdot (2 \cdot k + dk) \cdot dk$$

where s is the ratio of the length of the bending portion to the bar length and de_R is the increment of the normalized axial strain of straight segments.

$$de_R = dn/\mu_R = \{(C_1 \cdot \bar{A} + \rho \cdot \bar{S}) \cdot dk + \frac{C_2 \cdot \bar{A} \cdot (dk)^2}{1 + C \cdot dk}\}/\mu_R \tag{6}$$

Computed results using the stress-strain relation, shown in Fig. 5, are compared with the experiments (3), in Figs. 6(a),(b). Both are in good agreement. The hysteresis loops obtained theoretically are composed of finite number of curves with corresponding branching points, and can be approximated, without loss of accuracy, by the piecewise linear relation composed of straight lines connecting each branching points.

RESPONSE ANALYSIS

Fig. 7 shows a part of the piecewise linear hysteresis loop. The ordinate denotes the ratio f of the restoring force F to the reference value F_o, and the abscissa corresponds to the ratio ξ of the relative displacement x to the reference value x_o. Let f_1 and g represent the non-dimensional restoring force and stiffness at time $\tau = \tau_1$, respectively. The equation of motion of the undamped system, in the vicinity of $\tau = \tau_1$, is written as

$$\frac{d^2\xi}{d\tau^2} + \omega_o^2 \cdot \{g \cdot d\xi + f_1 + \gamma \cdot \phi(\tau)\} = 0 \tag{7}$$

where ω_o denotes the circular frequency of the elastic vibration, $\phi(\tau)$ is the normalized ground accelerogram and γ is the ratio of the maximum ground acceleration to the yielding level (F_o/M_e).

If $\phi(\tau)$ is expressed by the p-th order power series of time increment t as $\phi(\tau_1 + t) = \sum_{r=0}^{p} a_r \cdot t^r$, the relative-displacement increment $d\xi$ and the velocity $\dot{\xi}$ at time $\tau = \tau_1 + t$ is obtained as

$$d\xi = \sum_{r=1}^{p} b_r \cdot t^r + b_o \cdot \{1 - \cos(\omega \cdot t)\} + b/\omega \cdot \sin(\omega \cdot t) \tag{8}$$

$$\dot{\xi} = \sum_{r=1}^{p} r \cdot b_r \cdot t^{r-1} + b_o \cdot \omega \cdot \sin(\omega \cdot t) + b \cdot \cos(\omega \cdot t) \tag{9}$$

where

$$b_r = \begin{cases} 0 & : \ r > p \\ -\{\gamma \cdot a_r + (r+2) \cdot (r+1) \cdot b_{r+2}/\omega_o^2\}/g & : \ 1 \leq r \leq p \end{cases}$$

$$b_o = -(f_1 + \gamma \cdot a_0 + 2 \cdot b_2/\omega_o^2)/g$$

$$b = \dot{\xi}|_{t=0} - b_1, \quad \omega^2 = \omega_o^2 \cdot g$$

Eqs. 8 and 9 are valid for finite time increment, provided that the sign of the velocity does not change, and that the displacement increment $d\xi$ does not exceed the necessary increment $d\tilde{\xi}$ for the stiffness change, shown in Fig. 7. If one of these conditions is violated, substituting $d\xi$ or 0 to the left member of Eqs. 8 and/or 9, and solving it, the necessary time increment is obtained for the subsequent stiffness change and/or unloading. At the point of the stiffness change or the unloading, calculating the stiffness and the subsequent point of the stiffness change, the step-by-step computation should be continued.

COMPUTED RESULTS AND DISCUSSIONS

The load-displacement relation under monotonic loading is illustrated by the solid line in Fig. 8, assuming that the hysteretic characteristics of the bare frame is bi-linear with hardening ratio μ_f, and that the restoring force of the total system is evaluated by the simple summation of the restoring forces of each structural elements. In the figure, components of the restoring force shared by each structural elements are also illustrated by dashed line and dotted lines, defining the strength of the system with the brace of 0 length, $F_o = F_{fo} + 2 \cdot F_{bo}$, and the corresponding displacement x_o as the reference values, respectively. It is also assumed that the displacement at which the column attains its yield limit is twice the displacement at which the tension brace yields.

In Fig. 9, the computed results of the response analysis to the El Centro 1940 NS accelerogram at which the brace-restoring forces are evaluated by the proposed restoring-force function are compared with the precise solution where they are calculated through the detailed numerical procedure. The fundamental period is set as $T = 0.5$ sec., the ratio of the maximum acceleration of the ground input to the yield level of the system as $\gamma = 2$, the hardening ratio of the bare frame as $\mu_f = 0.05$, the slenderness parameter of braces as $n_E = 1$, and the ratio of the strength of the bare frame to the reference strength as $\alpha_f = F_{fo}/F_o = 0$, 1/5 and 1/2. The shape of the hysteresis loop much depends on α_f, and the response is also dependent on α_f. The results at which the brace-restoring forces are evaluated by the proposed function are in agreement with the precise solutions, and the deviations are very small if $\alpha_f \geq 1/5$. Therefore it is confirmed that the proposed restoring-force function of a single brace can be applied with enough accuracy to the dynamic response analysis of braced frames.

In Figs. 10 - 13, the results of a parametric study using the proposed hysteresis function of brace are shown. Fig. 10 shows the hysteresis for $n_E = 1$, 4, $\mu_f = 0$, 0.1 and $\alpha_f = 0$, 1/5, 1/3, 1/2, 2/3, 4/5, respectively. The other parameters and the input ground motion are the same as the case of Fig. 9. $n_E = 1$ approximately corresponds to the slenderness ratio $\lambda = 90$ and $n_E = 4$ to $\lambda = 45$ for mild steel. The shape of the hysteresis loop depends not only on n_E but also on α_f, and the dynamic response much depends on the hysteretic characteristics. For $\alpha_f \leq 1/2$, the hysteresis loop and the dynamic response are mainly dependent on n_E and the effect of μ_f is little. For larger values of α_f, the characteristics of the bare frame predominates and the effect of μ_f plays an important role. In the case of $n_E = 1$, the deformation drifts in the negative direction for $\alpha_f \leq 1/5$, and for $\alpha_f = 1/2$ the deformation is almost symmetric with respect to the origin and the maximum response takes the minimum. For $\alpha_f \geq 2/3$, the influence of the characteristics of the bare frame dominates, and the shapes of the hysteresis loops are similar to the bi-linear type, but the maximum response is larger than that for $\alpha_f = 2$. In the case $n_E = 4$, the deformation is almost symmetric with respect to the origin for small values of α_f and the drift of the deformation in the negative direction is observed for large α_f values. The maximum response takes the maximum for $\alpha_f = 1/2$. For $\alpha_f \geq 2/3$, as the effect of the bare frame predominates, the hysteresis loop and the response characteristics are similar to the case of $n_E = 1$.

Fig. 11 shows the relationship between the ductility responses of braces $\zeta_b = |x|_{max}/x_{bo}$ and α_f, and corresponding load-displacement relations under monotonic loading are shown in Fig. 12. The thin dotted lines in Fig. 11 denotes the response of the elastic-perfectly plastic system, and the deviation of the present results from these lines denotes the influence of the hysteretic charcteristics. The ductility response of a column is one half of that of the brace. The other parameters and input ground motion are the same as the case of Fig. 10. If the slender braces are used (n_E = 0.5 or 1), ζ_b decreases monotonically with the increase of α_f for $\alpha_f \leqq 1/2$. For large values of α_f, ζ_b becomes uniform at $\mu_f = 0.1$, but in the case of $\mu_f = 0$, ζ_b takes larger value than for $\alpha_f = 1/2$, although the load-displacement relation under monotonic loading shows more favourable shape for $\alpha_f = 2/3$ or $4/5$ than for $\alpha_f = 1/2$. In the case of $n_E = 2$ and/or 4 ζ_b takes the maximum in the vicinity of $\alpha_f = 1/2$, and for $n_E = 4$, ζ_b becomes small with small values of α_f. In the case of $n_E = \infty$, the hysteretic property of the brace is assumed to be bi-linear and the total behavior is tri-linear, as shown in Fig. 12(f). The effect of μ_f comes at its maximum at $\alpha_f = 2/3$, and is almost negligible for $\alpha_f \leqq 1/2$ and $n_E \leqq 2$.

ζ_b vs. n_E relations are shown in Fig. 13. In the case of $\alpha_f \leqq 1/3$, ζ_b becomes large for small n_E, and this tendency is remarkable for small α_f value. In the case $\alpha_f = 1/2$, ζ_b takes the maximum at $n_E = 4$, on the contrary ζ_b values at $n_E = 4$ are very small for $\alpha_f \leqq 1/2$. In the case $\alpha_f = 2/3$ and $4/5$, ζ_b increases with the decrease of n_E for $n_E \geqq 2$, and ζ_b takes almost constant value for $n_E \leqq 1$.

CONCLUSIONS

Dynamic response analysis of a single-story braced frame is presented. The hysteretic characteristics of the bare frame is assumed to be bi-linear, and the restoring-force of braces is evaluated by the hysteresis function proposed by the author and others and/or computed by the detailed numerical method. Both results are in good agreement, and it is confirmed that the proposed restoring-force function of a single brace can be applied to the response analysis with enough accuracy.

A parametric study using the proposed function shows: 1) The ductility response of the braced frame depends not only on the brace slenderness factor n_E but also and much on the strength factor α_f of the bare frame portion. 2) Although the load-displacement relation of a braced frame under monotonic loading shows favourable tendency for large values of n_E and α_f, the ductility responses often become large for rather large values of n_E or α_f. 3) Slender braces are inappropriate for structures with small α_f values, where the earthquake resistant property much depends upon braces.

REFERENCES

1. Wakabayashi, M., Nakamura, T., Shibata, M., Yoshida, N. and Masuda, H., 1977, "Hysteretic Behavior of Steel Braces Subjected to Horizontal Load Due to Earthquake", Proc. 6 WCEE, New Delhi, pp. 3188-3193.
2. Shibata, M., "An Analysis on Elastic-Plastic Behavior of Steel Braces", to be published.
3. Shibata, M., Nakamura, T., Yoshida, N., Morino, S., Nonaka, T and Wakabayashi, M., 1973, "Elastic-Plastic Behavior of Steel Braces under Repeated Axial Loading", Proc. 5 WCEE, Rome, pp. 845-848.

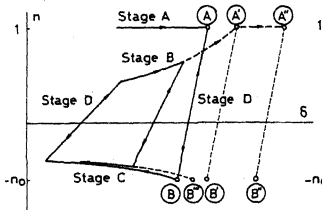

Fig. 1. Hysteretic rule.

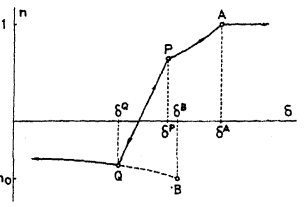

Fig. 2. Current n - δ relation.

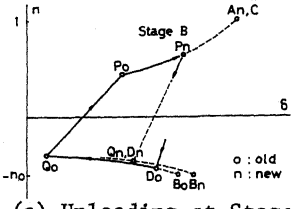

(a) Unloading at Stage B.

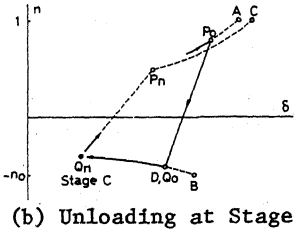

(b) Unloading at Stage C.

Fig. 3. Determination of characteristic points.

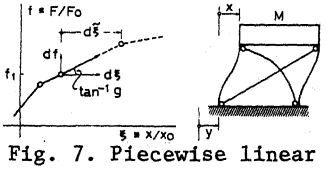

Fig. 7. Piecewise linear hysteretic characteristics.

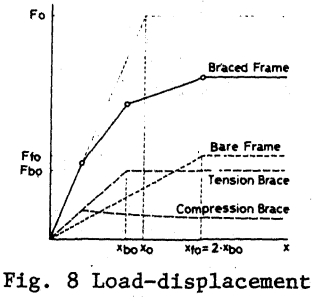

Fig. 8 Load-displacement relation under monotonic loading.

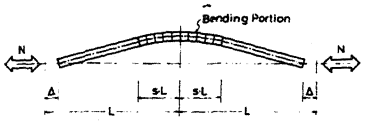

Fig. 4. Analytical model.

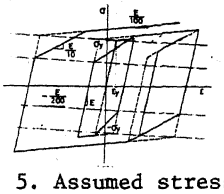

Fig. 5. Assumed stress-strain relation.

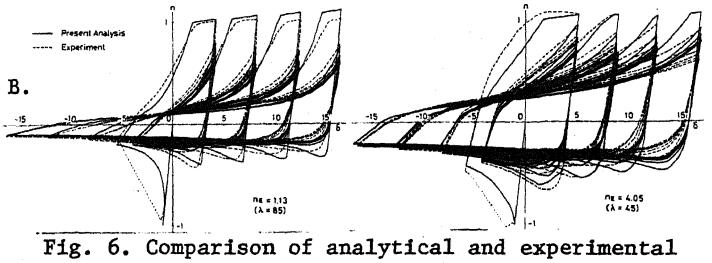

Fig. 6. Comparison of analytical and experimental results.

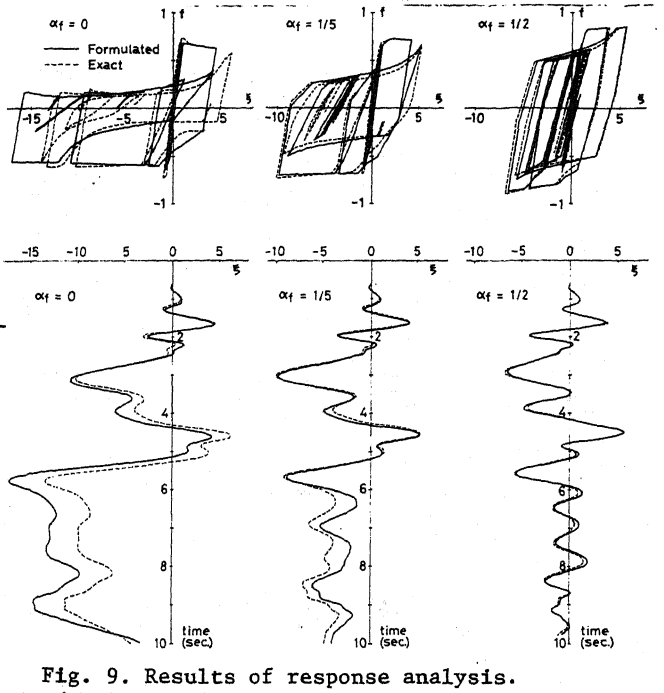

Fig. 9. Results of response analysis.

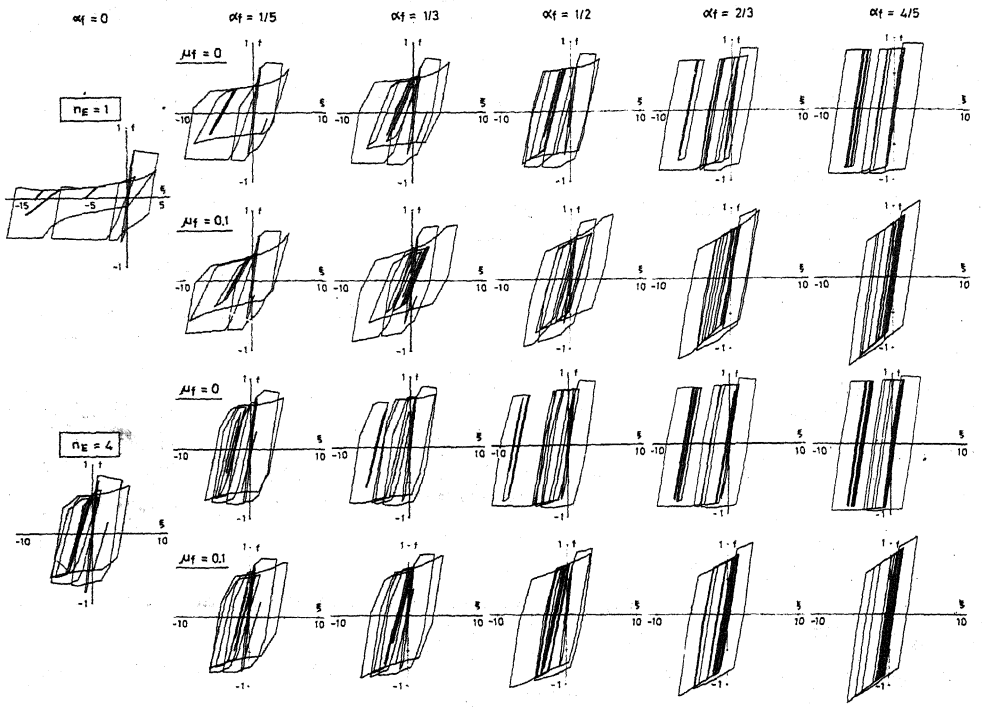

Fig. 10. Hysteretic load-displacement relations.

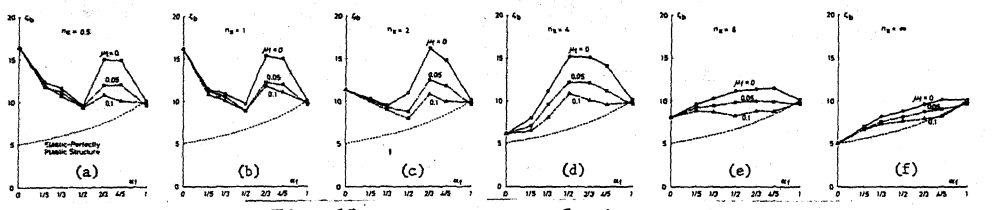

Fig. 11. ζ_b vs. α_f relations.

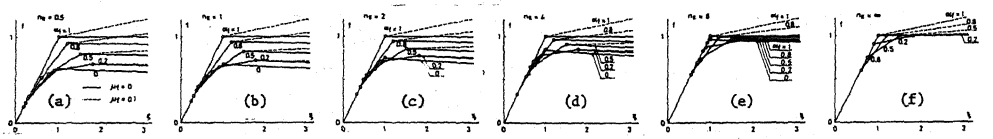

Fig. 12. Load-displacement relations under monotonic loading.

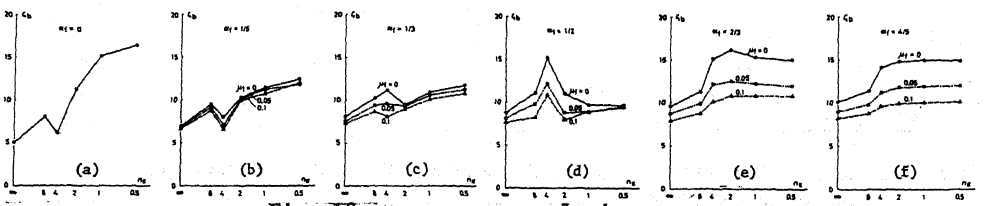

Fig. 13. ζ_b vs. n_E relations.